SANDIA REPORT
SAND2012-4750
Unlimited Release
Printed January 2013

Computational Model of Miniature Pulsating Heat Pipes

R. C. Givler and M. J. Martinez

Prepared by
Sandia National Laboratories
Albuquerque, New Mexico 87185 and Livermore, California 94550

Sandia National Laboratories is a multi-program laboratory managed and operated by Sandia Corporation, a wholly owned subsidiary of Lockheed Martin Corporation, for the U.S. Department of Energy's National Nuclear Security Administration under contract DE-AC04-94AL85000.

Issued by Sandia National Laboratories, operated for the United States Department of Energy by Sandia Corporation.

Available to DOE and DOE contractors from
U.S. Department of Energy
Office of Scientific and Technical Information
P.O. Box 62
Oak Ridge, TN 37831

Telephone: (865) 576-8401
Facsimile: (865) 576-5728
E-Mail: reports@adonis.osti.gov
Online ordering: http://www.osti.gov/bridge

Available to the public from
U.S. Department of Commerce
National Technical Information Service
5285 Port Royal Rd.
Springfield, VA 22161

Telephone: (800) 553-6847
Facsimile: (703) 605-6900
E-Mail: orders@ntis.fedworld.gov
Online order: http://www.ntis.gov/help/ordermethods.asp?loc=7-4-0#online

SAND2012-4750
Unlimited Release
Printed January 2013

Computational Model of Miniature Pulsating Heat Pipes

M. J. Martinez and R. C. Givler
Engineering Sciences Center
Sandia National Laboratories
P.O. Box 5800
MS0836
Albuquerque, New Mexico 87185

Abstract

The modeling work described herein represents Sandia National Laboratories' (SNL) portion of a collaborative three-year project with Northrop Grumman Electronic Systems (NGES) and the University of Missouri to develop an advanced, thermal ground-plane (TGP), which is a device, of planar configuration, that delivers heat from a source to an ambient environment with high efficiency. Work at all three institutions was funded by DARPA/MTO; Sandia was funded under DARPA/MTO project number 015070924. This is the final report on this project for SNL.

This report presents a numerical model of a pulsating heat pipe, a device employing a two phase (liquid and its vapor) working fluid confined in a closed loop channel etched/milled into a serpentine configuration in a solid metal plate. The device delivers heat from an evaporator (hot zone) to a condenser (cold zone). This new model includes key physical processes important to the operation of flat plate pulsating heat pipes (*e.g.* dynamic bubble nucleation, evaporation and condensation), together with conjugate heat transfer with the solid portion of the device. The model qualitatively and quantitatively predicts performance characteristics and metrics, which was demonstrated by favorable comparisons with experimental results on similar configurations. Application of the model also corroborated many previous performance observations with respect to key parameters such as heat load, fill ratio and orientation.

ACKNOWLEDGMENTS

The modeling work described herein, was part of a joint project among Northrop Grumman Electronic Systems (NGES), the University of Missouri and Sandia National Laboratories. It was funded by DARPA/MTO, proposal number 015070924. We acknowledge many beneficial discussions with our collaborators at these institutions: Larry Greenberg and Rob Young at NGES and Prof. Hongbin Ma and his students at Mizzou.

We also note the many helpful discussions with Melissa Carter, Harry Chen, Anurag Chandorkar and Tony Hirt, all of Flow Science Inc., during the development of the flow model with free boundaries.

The views expressed are those of the authors and do not reflect the official policy or position of the Department of Defense or the U.S. Government.

Approved for Public Release, Distribution Unlimited.

CONTENTS

FIGURES

TABLES

NOMENCLATURE

2D	two space dimensions (x,y)
3D	three space dimensions (x,y,z)
A	area
c	specific heat (J/kg-K)
C	effective accommodation coefficient
CHP	conventional heat pipe
e	specific energy (J/kg)
E	energy, (J)
F	volume of fluid indicator
g	gravity vector (m/s^2)
h	width (m)
h	heat transfer coefficient (W/m^2)
k	thermal conductivity (W/mK)
l	length (m)
L	latent heat (J/kg)
m	mass (kg)
M	molecular weight (gm/mole)
MTO	Microsystems Technology Office
NGES	Northrop Grumman Electronic Systems
SNL	Sandia National Laboratories
t	time (s)
T	temperature (K or C)
TGP	Thermal ground-plane
p	pressure (Pa)
PHP	pulsating heat pipe
Q	thermal power (W)
q	thermal power density (W/m^3)
R	gas constant (J/mol-K)
u	velocity vector (m/s)
u,v	components of velocity (m/s)
$\bar{u}$	time-averaged value for *u*
V	volume
w	thickness (m)
x	volume fraction

Greek symbols

ρ	density (kg/m^3)
θ	contact angle (radians)
τ	viscous stress tensor (Pa)

Superscripts and Subscripts

bdy	boundary
cond	condenser

eff	‘effective’
evap	evaporator
init	initial
l,liq	liquid
s	solid
sat	thermodynamically saturated condition
surf	surface
v, vap	constant volume, vapor
0	initial value, baseline

EXECUTIVE SUMMARY

Northrop Grumman Electronic Systems (NGES), the University of Missouri, and Sandia National Laboratories (SNL) collaborated on a three-year, multi-faceted program to develop an advanced thermal ground-plane (TGP). A well-designed thermal ground-plane is any device, of planar configuration, that transports heat from a source to an ambient environment with high efficiency. Activities at all three institutions were funded by DARPA/MTO.

SNL was tasked with model development to help direct the design of highly-efficient TGPs. This report summarizes SNL's portion of the total project. Our objective was to gain a working knowledge of pulsating heat pipes (PHPs) through the development of a comprehensive model; application of this model gave insight as to how PHPs operate and how various parameters (geometrical configuration, fill ratio, materials, working fluid, orientation, *etc.)* affect thermal performance. Also, in contrast to existing models that mostly consider tubular designs, we consider PHPs milled or etched into a solid substrate as a prototypical design for cooling of electronics.

The physical processes at play for a working PHP are highly coupled. Understanding PHP operation is further complicated by the dynamic interplay between evaporation/condensation, bubble growth and collapse or coalescence, and the coupled response of the two-phase fluid dynamics among adjacent channel segments. This report documents results of an improved numerical model for a PHP featuring a two-phase (liquid and its vapor) working fluid confined in a closed-loop, serpentine channel etched in a solid copper plate. Our modeling approach utilizes the FLOW-3D software (Flow Science, 2007). This new model includes relevant physical processes common to the operation of any flat plate PHPs: two-phase heat, mass and momentum conservation including dynamic bubble nucleation, evaporation and condensation with latent heat effects, together with conjugate heat transfer with the etched substrate. Thus, for the first time, the behavior of a working PHP can be accurately modeled. The model describes qualitatively and predicts quantitatively performance characteristics and metrics; this was demonstrated by favorable comparisons with experimental results on similar configurations, discussed in Section 3 below. Application of the model also corroborated previously observed behavior with respect to key parameters such as heat load, fill ratio and orientation. This work advances the state-of-the-art for modeling PHPs.

1. INTRODUCTION

A heat pipe is a passive device that *enhances* the transfer of heat from a region of higher temperature (*i.e.* evaporator) to a region of lower temperature (*i.e.* condenser). Typically, a heat pipe employs a working fluid confined within a sealed channel/compartment, in which the working fluid cycles between its liquid and vapor states during heat pipe operation. The latent heat associated with this change-of-phase greatly improves the efficiency of the device. Heat pipes were developed in the 1960's, motivated by the space program, as a passive device (no external energy supply is required) capable of high heat transfer rates. Ever-increasing power densities in semi-conductor electronics continue to motivate improvements to heat pipe design. A typical configuration for a conventional heat pipe (CHP) is a sealed tube in which the cross sectional flow area is partially occupied by a wick structure, usually attached to the tube walls, while the remainder of the flow area is open. At the evaporator, the heat injected promotes liquid evaporation, thereby reducing the moisture content in the wick and raising the local vapor pressure, which drives vapor towards the condenser via the open flow area. At the cooler condenser, vapor condensation raises the moisture content in the wick and releases its latent heat. The wick plays a crucial role in the operation of CHPs; it moves liquid, via a capillary pressure gradient, from the relatively wet condenser to the relatively dry evaporator. Critical to this cycle of continuous operation is the ability of the wick to supply sufficient liquid to the evaporator. In cases where a CHP is subject to high heat flux loadings the wick may be unable to supply sufficient flow of liquid to the evaporator prompting a 'dry-out' condition, meaning all liquid has been evaporated, leaving only a superheated vapor. In these instances, the heat pipe cycle loses the latent heat effect for energy transfer, causing the evaporator temperature to rise sharply and the performance of the heat pipe to decline. The consequence of this sequence of events can be dramatic; the heat-producing device, which the CHP was dedicated to protect, will overheat and may subsequently fail. This so-called "wicking limit" provides a functional, limiting, relationship between the maximum heat flux (power) and CHP length, for a given wick, which the heat pipe can achieve without dry-out. Thus, much of the research dedicated to the advancement of CHPs has been in the area of wick design. Exotic wick designs can add construction expense. CHPs are thus limited by wick design, the rate of heat transfer and the distance over which they can perform.

Pulsating heat pipes (PHP's, also called oscillating heat pipes or OHP's) have been proposed as an alternative to CHP's; an important distinction is that a wick is not required. A common design for a PHP is a capillary-sized tube or channel forming a closed, continuous flow loop and containing a liquid and its vapor. The flow loop is configured in a serpentine fashion, with many back-and-forth legs, resulting in a typically rectangular planform, which is heated at one end (evaporator), while cooled at the opposite end (condenser), *e.g.* Figure 1. If the capillary diameter is not too large, the fluid distributes itself into an arrangement of liquid slugs separated by vapor bubbles (often referred to as plugs). During operation, heat input to the evaporator expands existing bubbles and/or nucleates new bubbles, driving liquid and bubbles toward the cooler condenser region, where vapor bubbles contract or collapse via condensation. The evaporation/condensation cycle provides the motive force for the convective motion, though heat

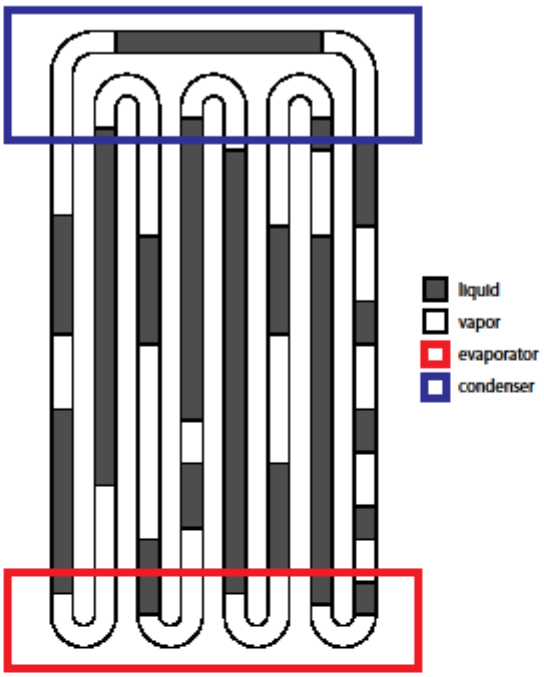

Figure 1: Schematic of a bottom-heated, 4-turn, single-loop PHP.

Figure 1. Schematic of a bottom-heated, 4-turn, single-loop PHP.

is mainly transferred sensibly by the movement of hot liquid from evaporator to condenser. These devices are called "pulsating" heat pipes because the evaporation/condensation process happens as a non-equilibrium episodic/chaotic process, whose continuous operation requires non-equilibrium conditions to exist in some, but not necessarily all, of the parallel channels at any given instant of time. As with CHPs, no external power source is needed to either initiate or sustain the fluid motion or the transfer of heat.

Compared to CHPs, the absence of a wick in a PHP results in several attractive features: (*i.*) PHPs are simpler and cheaper to construct because exotic wick structures are not required, (*ii.*) pressure losses associated with liquid flow through the wick structure are eliminated, and (*iii.*) higher heat fluxes are possible with the elimination of limitations associated with wick-limiting dry-out.

PHPs were invented by Akachi (1990), as disclosed in a U.S. patent, and investigations by him and his co-workers continued during the 1990's (Akachi *et al.*, 1996, Miyazaki and Akachi, 1996, 1998). His invention described a device made from small-bore tubing as described earlier. Akachi found that a check valve, used to promote uni-directional flow, improved performance. Concerted experimentation and analysis by other groups began *c.* 2000. Zuo *et al.* (1999 & 2001) prototyped a hybrid PHP which featured a sintered wick to enhance performance, and a copper prototype capable of dissipating up to 200 W/cm^2; they reported an optimal liquid fill ratio, x_{liq}, of about 0.70 for their device. Khandekar *et al.* (2002) considered a flat plate heat pipe with channels (rectangular cross section) that were milled into a thin aluminum plate; for comparison, they also constructed a PHP of parallel tubes connected by copper U-turns. They concluded that PHP operation is influenced by tilt-angle (with reference to the gravity vector), liquid fill ratio and cross-sectional dimensions. The rectangular channels promote a strong capillary force not found with circular tubes, because the liquid experiences enhanced wicking along the channel corners. They also suggest that heat transfer across adjacent flow channels can be detrimental to the maximum performance of the device. Khandekar and Groll (2004) considered a one-loop PHP experiment as a primary building block for a multi-turn PHP. They found: (*i.*) a number of distinct flow regimes that depend on the input power, (*ii.*) gravity has an effect on the liquid/vapor motion, and (*iii.*) oscillations stopped when the PHP is in a horizontal orientation. Moreover, they found a complete stop-over configuration, not previously noted in multi-turn loops, from which they inferred that more turns in the PHP architecture increases the number of flow perturbations and is necessary for the pulsating behavior. Experiments by Khandekar and co-workers (Khandekar *et al*., 2003a-c) have explored other aspects of PHPs. They report fill ratios between 25-65% are needed to observe pulsating behavior, and that device orientation with respect to gravity is important. Their findings also suggest a minimum number of turns are needed to improve device operation. In Khandekar *et al*., 2003c, they construct a qualitative map of flow regions observed with respect to inclination angle and heat load. Ma and co-workers have also conducted experimental studies of PHPs, especially with respect to the beneficial use of nanoparticles (Ma *et al*., 2006a, 2006b) and issues regarding device start-up (Qu and Ma, 2007). More recently, this group has recorded video images using neutron radiography of a working PHP (Wilson *et al*., 2008). Thompson *et al.* (2011a) report experimental measurements from a three-dimensional "flat" (i.e. channels formed in a solid substrate, as opposed to a tubular design) heat pipe with heat fluxes as high as 300 W/cm^2. Their

configuration utilized heating and cooling areas that sum to greater than 80% of the total planform area, which is impractical as a heat pipe device for long-range cooling applications.

Past modeling efforts are based on the idea of describing PHPs by a train of liquid slugs separated by vapor bubbles confined in a tube and then constructing control volume conservation relations for each discrete phase (Shafii *et al.,* 2001; Zuo *et al.*,2001; Zhang and Faghri, 2002; Zhang *et al.*, 2002; Zhang and Faghri, 2003, Yuan *et al.*, 2010). These models attempt to describe a variety of physical configurations and phenomena, including evaporation and heat conduction in the liquid slugs. Shaffii *et al*. considered both closed looped and open loop PHPs, and their model can accommodate many vapor bubbles and liquid slugs, although they show a majority of results for three bubbles. Typical of these mathematical models, they produce periodic variations in temperature and pressure from which one can calculate both angular frequencies of pulsation and the total heat transferred from evaporator to condenser; reported thermal efficiencies are less than those demonstrated by either Zuo *et al.* (2001) or Wilson *et al.* (2008). Zhang and Faghri (2002) describe a similar model, though they assume the vapor phase is saturated at all times, whereas Shaffii *et al.* construct a mass transfer model driven by the difference between the bubble and local wall temperatures. Nikolayev (2011) recently extended like models by proposing an evaporation rate based on an interfacial heat balance; a similar idea is applied in this work and described in Section 2.3. Nikolayev's model displays intermittent behavior as is seen in experimental visualizations, an improvement to the Zhang models which demonstrate strictly periodic behavior. Most modeling studies conclude that a majority of energy transferred by a PHP is by sensible heat, with latent heat effects providing the motive force for motion, but not responsible for much of the net heat transfer.

Although the models proposed to date include some relevant mechanisms for describing PHP operation, they also neglect a few. Most models are one-dimensional and comprised of coupled sub-models to represent bubbles and liquid slugs. In addition, they ignore heat transfer with the confining materials, be it tubing or solid substrate. None of the cited models consider bubble nucleation, possibly explaining why Shaffi predicted monotonic liquid slug coalescence even when starting out with many isolated slugs. Our own experience using the Zhang 'U-tube' model (Givler & Martinez, 2009) is that their treatment over-predicts typical pulsating frequencies and the heat balance is incomplete.

Although there have been many experimental and theoretical modeling studies of PHPs, the interplay of heat transfer and fluid mechanics is not well understood. Many of the conclusions drawn by various authors are inconsistent with each other. The objective of the present research is to develop a more complete multi-physics model for this complex phenomenon to assist with understanding how PHPs operate and how various parameters (geometrical configuration, liquid fill ratio, materials, working fluid, device orientation, *etc.)* affect its performance. Also, in contrast to existing models which mostly consider tubular designs, we consider PHPs milled or etched into a solid substrate, as a prototypical design for cooling electronics. The physical processes describing a PHP are highly coupled. Understanding its operation is further complicated by the non-equilibrium nature of the interplay between evaporation/condensation, bubble growth and collapse or coalescence, and the coupled response of the multiphase fluid dynamics among adjacent channels. A comprehensive theory of operation and design guidelines

for PHPs is still an unrealized task. Our aim in this paper is to advance the state-of-the-art for modeling PHPs and to address current deficiencies.

The remainder of this report is arranged as follows. In Section 2 we provide a mathematical description for a three-dimensional model, including details of the crucial aspects of evaporation, condensation and bubble nucleation. We describe our numerical model utilizing some unique features available in the commercial software FLOW-3D, version 9.2-3 (Flow Science, 2007). Section 3 presents numerical results from a full 3D model, which was used to justify further studies that employed a more computationally efficient 2D configuration. Next, we present results for the 2D pulsating heat pipe and explore its performance with changes to the number of turns, heat load, liquid fill ratio and orientation with respect to gravity. We also investigate the use of a Tesla-type valve, to promote circulatory flow. We close by summarizing the main findings of our model study.

2. NUMERICAL MODEL

2.1 Model Geometry

Figure 2 is a schematic of the baseline PHP configuration analyzed in this work. The PHP is constructed from a rectangular block of material in which a closed serpentine channel has been removed, either by milling or using an etching process. The evaporator region, located at one end of the device, is where heat is supplied and is modeled as a volumetrically heated region encompassing a portion of the channels. The condenser located on the opposite side of the device, is also modeled as a volumetric region. Heat is extracted by specifying that this region is maintained at fixed temperature, T_{cond}. The region between the condenser and evaporator is modeled as an adiabatic region, wherein the device is insulated from heat losses to the environment. The interior channel is filled with a two-phase working fluid, a liquid and its vapor. The model includes dynamic evaporation and condensation of discrete vapor bubbles as depicted in Figure 2. The liquid and vapor phases are treated discretely.

2.2 Liquid Phase

The conservation of mass and momentum in the liquid are described by the Navier-Stokes equations, written here for a single phase region of the flow problem:

$$\begin{aligned} &\frac{\partial \rho}{\partial t} + \nabla \bullet \rho \mathbf{u} = 0 \\ &\frac{\partial u}{\partial t} + \mathbf{u} \bullet \nabla \mathbf{u} = \frac{1}{\rho}\left[-\nabla p + \nabla \bullet \boldsymbol{\tau}\right] \end{aligned} \tag{1}$$

in which $\boldsymbol{\tau}$ is the viscous stress tensor. The conservation of energy is written in terms of internal energy,

$$\frac{\partial \rho e}{\partial t} + \nabla \bullet \rho \mathbf{u} e = -p \nabla \bullet \mathbf{u} + \nabla \bullet \left(k \nabla T\right). \tag{2}$$

To model free boundary flows in general, FLOW-3D utilizes a volume of fluid (TruVOF) scheme first introduced by Hirt & Nichols (1981). The idea is to track the liquid phase (in the present problem) with a function, $F(\mathbf{x},t)$, which plays the role of a volume indicator: $F = 1$ in regions which are fully occupied by the liquid phase, $F = 0$, in regions fully occupied by the vapor phase, and $0 < F < 1$ in regions (*i.e.* grid cells) that are partially filled with liquid (two-phase cells). The function, F, is convected according to,

$$V_F \frac{\partial F}{\partial t} + \nabla \bullet \left(F \mathbf{A} \bullet \mathbf{u}\right) = 0 \tag{3}$$

where V_F is the fractional volume open to flow, and $\mathbf{A} = \mathrm{diag}(A_x, A_y, A_z)$ represents the fractional area open to flow along each coordinate direction. The fractional volume and area enable the description of flow in cells that are two-phase, *i.e.*, occupied by both liquid and its vapor. These fractional values are included in the conservation equations for two-phase cells, otherwise their values are unity in single phase liquid cells. Spatial gradients of the function, F, can be used to

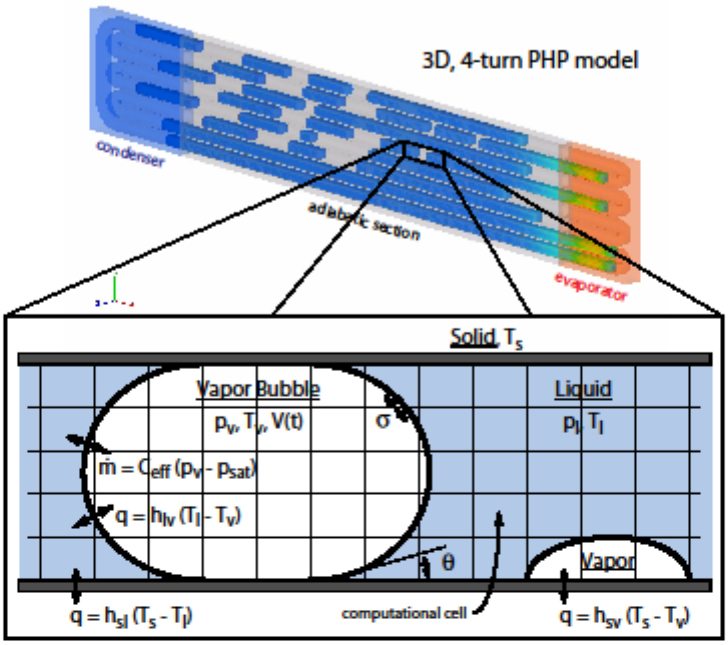

Figure 2: A schematic identifying the participating interfacial physics and defining relevant model parameters.

Figure 2. A schematic identifying the participating interfacial physics and defining relevant model parameters.

construct a representation of the free surface when surface tension between the phases is important, as it is here.

Compared to the more recently developed and rival Level Set interface tracking scheme (Sethian 1999, Osher & Fedwick 2003), TruVOF generally provides more accurate mass conservation in free boundary flow problems.

2.3 Homogeneous Bubble Model

Although FLOW-3D is able to treat general two-phase problems, in which the equations of motion are solved in each discrete phase, the present vapor/liquid flow problem can be effectively treated by taking advantage of the large contrast in density and viscosity between the phases. The dynamics of the vapor bubbles can be simulated using a "homogeneous bubble model" available in FLOW-3D. The key assumption in this sub-model is that both the (time-dependent) pressure, $p_v(t)$, and temperature, $T_v(t)$, within each bubble is spatially uniform. This is a good approximation for a vapor bubble of much lower viscosity and density than its corresponding liquid phase. Bubble evolution is described in terms of individual bubble heat, mass and momentum conservation equations which account for heat and mass exchange between a bubble and its surrounding, including energy exchange with solid objects exposed to the bubble. Each bubble must occupy at least a portion of one computational grid cell, but can span as many cells as required by the current bubble volume, $V(t)$. Many bubbles can be simultaneously modeled, and bubbles can disappear through condensation or coalescence and new bubbles can form based upon a cavitation criteria. A bubble is nucleated when the local pressure in the liquid falls below the saturation pressure at the prevailing temperature, $p < p_{sat}(T_l)$. A positive value of superheat can be specified, which allows the bulk liquid to heat that many degrees before vapor bubbles are nucleated. We did not specify a value of superheat in these simulations. For reasons related to numerical stability, FLOW-3D allows the specification of a characteristic time for bubble formation, in terms of a number of time steps over which the bubble transitions from nucleation to a homogeneous thermal bubble. The equation of state for the vapor is approximated by the ideal gas law,

$$p_v = \rho_v R T_v / M \tag{4}$$

where p_v is the bubble pressure, ρ_v is its density, T_v is the vapor temperature, R is the universal gas constant and M is the molecular weight of the vapor. One advantageous and distinguishing feature of the homogeneous bubble model is that it allows for the possibility of non-equilibrium thermodynamic conditions, meaning the vapor pressure in the bubble does not have to equal the saturation pressure at the prevailing temperature, as is commonly assumed (*e.g.* Plesset & Prosperetti, 1977, Zhang & Faghri, 2002). This is important for modeling fast temporal dynamics, which are expected during the operation of PHPs. This non-equilibrium condition, motivated by kinetic theory, is modeled by the following expression that describes the rate of mass transfer between liquid and its vapor (Hirt, 2001) *viz.*,

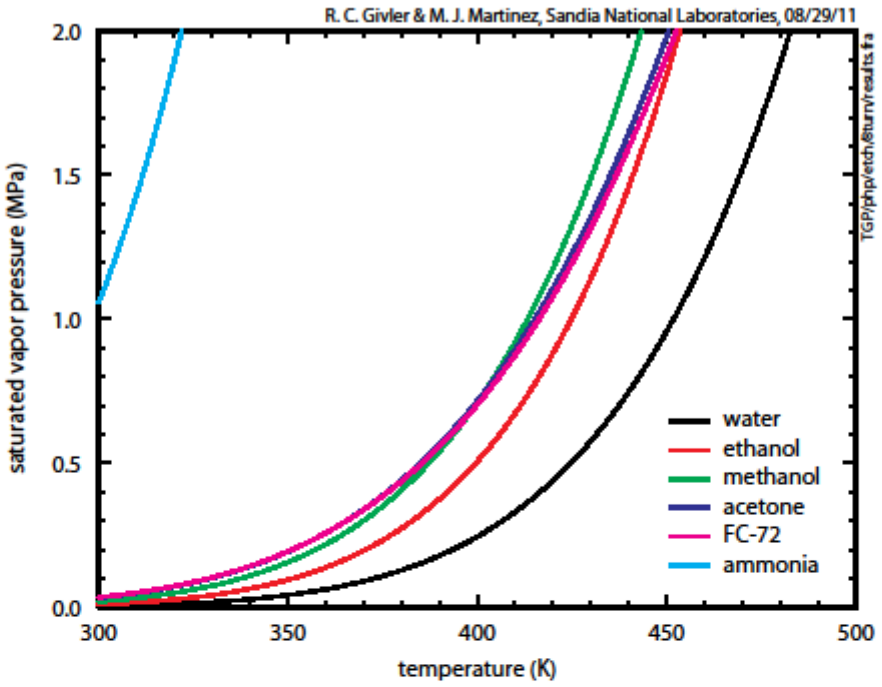

Figure 3: Vapor pressure variation with temperature for various working media.

Figure 3. Vapor pressure variation with temperature for various working media.

$$\dot{m} = C\sqrt{\frac{M}{2\pi R T_{bdy}}}\left(p_{sat}(T_l) - p_v\right) \tag{5}$$

Here p_{sat} is the saturated vapor pressure, evaluated at the local liquid temperature T_l and p_v is the vapor pressure in the bubble, as depicted in Figure 2. The saturated vapor pressure as a function of temperature is approximated by the Clapeyron equation (*e.g.* Callen, 1960). Figure 3 compares the saturated vapor pressures for several common working fluids. The parameter *C* is the net accommodation coefficient. Because the mass transfer model is motivated by kinetic theory, the accommodation coefficient can be interpreted as a probability that vapor molecules striking the liquid surface are captured. In the present work this value was set to 0.01, a value recommended by FLOW3D literature. Early sensitivity studies on simpler systems showed the results to depend weakly with variations about this value (Givler and Martinez, 2009). T_{bdy} is the average temperature of the surrounding liquid surface, computed in the following way,

$$T_{bdy} = \int T_l \, dS_{surf} \,/ \int dS_{surf} \,, \tag{6}$$

in which dS_{surf} is an element of surface area on the liquid/vapor interface. This average temperature is used in the bubble mass transfer model and is also the bubble temperature used to compute the internal energy of the bubble. The bubble can also exchange heat with solid surfaces that form a portion of its boundary, via a user-specified heat transfer coefficient. This results in a heat flux, $h_{sv}(T_s - T_v)$, where T_s is the local solid boundary temperature. Thus, the thermal bubble model is defined so that it respects limiting cases of adiabatic behavior: (*i.*) in the absence of energy exchange, and (*ii.*) it allows heat exchange in the absence of phase changes. The energy transfer to the liquid phase in the presence of a mass exchange Δm (from the mass transfer model) in a computational element is,

$$\Delta E = \Delta m \begin{cases} L + e_l & \text{if } \Delta m \geq 0 \\ L + c_v^{vap} T_v & \text{if } \Delta m < 0 \end{cases} \tag{7}$$

where L is the latent heat and $e_l(T_l)$ is the specific energy of the liquid at the local liquid temperature. In non-equilibrium situations, where the energy transferred in a time step exceeds the energy required to evaporate or condense Δm, the excess energy goes to heat the liquid upon condensation or cool the liquid upon evaporation. In general, the model remains close to equilibrium during most of the simulation. Only in instances with rapid transients would the non-equilibrium effects come into play. However, these cases can arise during the intermittent behavior of PHPs associated with bubble nucleation events.

FLOW-3D accounts for conjugate heat transfer in the solid regions that share common boundaries with the fluid. The solid regions exchange heat with the liquid via a user-specified heat transfer coefficient according to $h_{sl}(T_s - T_l)$.

3. RESULTS AND DISCUSSION

This section presents results for several simulations that demonstrate the performance of a PHP model for various operating conditions.

3.1 3D, 4-Turn, PHP Simulation Results

We begin by illustrating the dynamic response of a three-dimensional, 4-turn, PHP; this configuration represents a *baseline* model that features all relevant physics-based behavior available in the FLOW-3D software. The size of the device, and its channel dimensions, are typical of those that might result from a common industrial top-side, wafer-etching process; in practice, the open channels can be sealed by bonding a thin, top plate to the etched substrate. The overall dimensions of this device (depicted in Figure 4) are defined as follows: length, l, is 6.39 cm, thickness, w, is 0.162 cm and width, h, is 1.044 cm. The evaporator section (shaded in red on the right hand side of the PHP) measures 0.81 cm in length. Total heat, Q, generated within the copper that comprises the evaporator was 39.58 W. This corresponds to a volumetric heating rate of 441 MW/m^3, and a device heat flux load of Q/A = 234 W/cm^2, A being the device cross sectional area. This is the overall heat flux load dissipated by the device. Alternatively, the condenser section (shaded in blue on the left hand side of the PHP) measures 1.08 cm in length. The temperature of the copper substrate comprising the condenser was maintained at constant temperature, 298K, during the entire simulation. This was accomplished by prescribing an initial temperature, T_0 = 298 K, to the condenser and artificially assigning a large numerical value for the heat capacity, $c_p = 1e12$, of the copper substrate that defines the condenser. Relative sizes for the evaporator and condenser sections can affect the performance of a PHP. For example, if the condenser is too small the working fluid will not have sufficient residence time to dump its heat as it courses through the condenser. This will cause PHP performance, as measured by an effective thermal conductivity for the device, to suffer and we have, indeed, witnessed this behavior with our synthetic model. We have not tried to optimize PHP performance by right-sizing the heating/cooling sections for this PHP. Rather, we chose what we thought were reasonable sizes for these components in order to conduct an associated parametric study. Finally, the length of the adiabatic section, l_0, measures 4.5 cm; operationally, no heat is transferred to/from the environment within this section of the model. In fact, this can be said for the entire device, *i.e.* all external surfaces are insulated.

The serpentine channel that allows circulation of both liquid and vapor has a square cross-section measuring 0.9 mm per side. Five grid cells were assigned along each cross-length of the channel, resulting in 25-cell resolution on the channel cross-section. Two grid cells were assigned to the metal separating each channel. The time integration method utilized in this work is a Courant-limited automatic time stepping scheme. These simulations were computationally intensive and very time consuming hence prohibiting mesh refinement studies. The initial liquid fill fraction for the model shown in Figure 4 is 0.63; the working medium was water and its vapor. The device is bottom-heated, in that, the gravity vector is directed toward the evaporator. The initial temperature of the device and its contents were all set to 298K. All remaining material properties and run-time parameters can be referenced in Tables 1 and 2. In addition to boundary and initial conditions, Table 2 reports user-specified heat transfer coefficients for heat exchange between

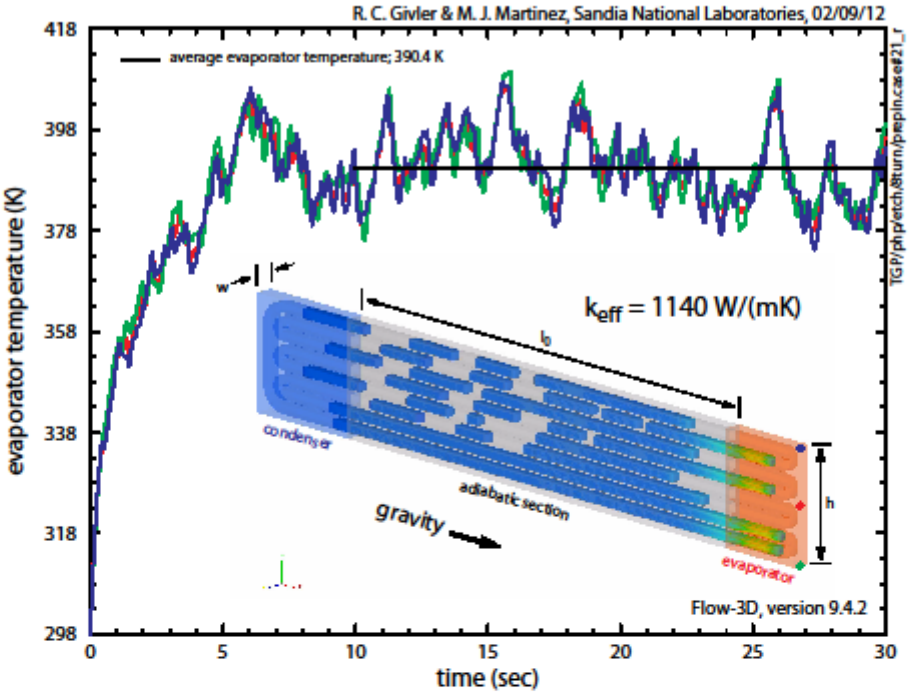

Figure 4: 3D, 4-turn, PHP simulation results.

Figure 4. 3D, 4-turn, PHP simulation results.

Table 1. Material Properties (Baseline Case)

	ρ (kg/m^3)	c_p (kJ/kg/K)	k (W/m/K)	σ (N/m)	α (degrees)	μ (kg/m/s)	$L_{vap/cond}$ (kJ/kg)
water (liq)	1000	4.182	0.597	0.07	120	0.001	2257
water (vap)	0.804	1.41	n.a.	n.a.	n.a.	n.a.	2257
acetone (liq)	793	2.16	0.160	0.025	120	0.0003	540
acetone (vap)	2.59	1.33	n.a.	n.a.	n.a.	n.a.	540
copper	8890	0.388	385	n.a.	n.a.	n.a.	n.a.

Table 2. Initial and Boundary Conditions

	T_{init} (K)	P_{init} (Pa)	h_{sl} ($W/m^2/K$)	h_{sv} ($W/m^2/K$)	q (MW/m^3)
evaporator	298	n.a.	30000	1000	441
connecting region	298	n.a.	30000	1000	n.a.
condenser	298	n.a.	30000	1000	n.a.
Water (liquid)	298	3727.1	30000	n.a.	n.a.
Water (vapor)	298	3727.1	n.a.	1000	n.a.

the liquid and solid, and between vapor and solid. The values specified are in the range of values measured for boiling in microchannels, as reported by Cheng *et al.* (2007).

Evaporator temperature is plotted as a function of time in Figure 4. The three separate temperature traces correspond to specific locations within the evaporator section. The location of each temperature trace is defined by the location of the corresponding colored dot along the evaporator edge (see device depiction in the figure inset). The temperature traces demonstrate some independence based upon their location. This behavior is a consequence of the intermittent liquid slug flow in the evaporator channels along with the associated boiling events. Both of these effects will produce local variations in evaporator temperature.

The figure inset displays the arrangement of liquid slugs within the device shortly after the simulation has begun (specifically $t = 0.075$ s). Temperature data indicate an initial transient (0 s $< t <$ 10 s) that gives way to oscillatory behavior after approximately 10 sec. We are most interested in the average temperature of the evaporator after the device has reached quasi-steady operation. The figure displays the time-averaged value for the evaporator temperature between 10 s $< t <$ 30 s that was calculated to be 390.4K. This quantification of the evaporator temperature permits one to compute an effective thermal conductivity, defined as,

$$k_{eff} = \frac{Ql_0}{A(T_{evap} - T_{cond})} \tag{8}$$

which for this device is 1140 W/(mK). Here, Q is the evaporator power, l_0 is the length of the adiabatic section, A is the cross-sectional area of the adiabatic section *i.e.* $w \times h$, T_{evap} is the time-averaged evaporator temperature and T_{cond} is the condenser temperature. For comparison, this value is 2.9 times that of a solid copper plate. This predicted performance is noteworthy given the fact that this improvement in transfer of heat was achieved with only 38% of the device cross-section acting as a PHP; the other 62% of the device cross-section was already copper substrate transmitting heat via thermal conduction.

Thompson *et al.* (2011b) report $k_{eff} \approx 700$ W/mK for a similar copper-substrate device of dimensions 3x3x0.254 cm^3 with square channels measuring 0.76 mm on a side. Zuo *et al.* (2001) report thermal resistances in the range of 0.15 – 0.6 ($^oC/W/cm^2$) for a similarly sized flat heat pipe, though the details of the number of turns and dimensions of the serpentine channel was not reported. The equivalent thermal resistance from our model for the present simulation is 0.395, in the same range as Zuo *et al.* The paper by Thompson *et al.*, (2011a), utilizing a stacked design with two layers of channels (0.76 mm hydraulic diameter) through the device thickness, also report thermal resistance values, albeit in units of $^oC/W$. However, as noted in Section 1, the evaporator and condenser took up the entire planform on this device, such that there is no adiabatic section ($l_0 = 0$). Hence, it is difficult to compare these results with our model as their device was not configured as a true heat pipe. Nevertheless, utilizing the device cross sectional area and the distance between the centroid of the heated and cooled regions as a surrogate for l_0, their results imply k_{eff} on the order of perhaps 2000 to 3000 W/mK. Thus, our numerical model is seen to produce performance metrics similar to those measured by experimentation, providing some validation for the quantitative predictions of this model.

3.2 2D, 4- and 8-Turn PHP Simulation Results

The 3D simulation discussed in the preceding section was computationally intensive and, thus, very time consuming to perform. For that reason, we decided to conduct the remaining parametric study using 2D renditions of thin, etched-channel PHP's. But first, it is instructive to compare the performance from a 2D model with that of its 3D counterpart discussed in the previous section. From this exercise, one can gain confidence in using 2D model simulations to draw conclusions about PHP performance.

Simulation results for a two-dimensional, 4-turn, PHP are illustrated in Figure 5. This model represents a slice through the mid-plane of the 3D model of Section 3.1. All aspects of the 2D model are either functionally identical to or scaled appropriately to those of the 3D case with the exception of the 'through-the-thickness' dimension. Geometrically this means that there is an under-accounting of copper cross-section in the adiabatic region of the 2D model as compared with its 3D counterpart. In addition, total amount of heat transfer between liquid/vapor and the channel walls will be reduced in the 2D model, again owing to a reduction in equivalent surface area. Consequently, one would expect the value for k_{eff} predicted by the 2D model to be somewhat lower than that reported for the 3D model. Upon inspection of the results presented in Figure 5, this is indeed the case. The time-dependent evaporator temperature is illustrated by the non-steady black curve; its quasi-steady 'average temperature' (obtained from three separate edge locations) is also plotted with a computed value of 378.1 K. In turn, k_{eff} is calculated to be 761 W/(mK). The baseline device heat load is 135 W/cm^2. Despite the lower performance

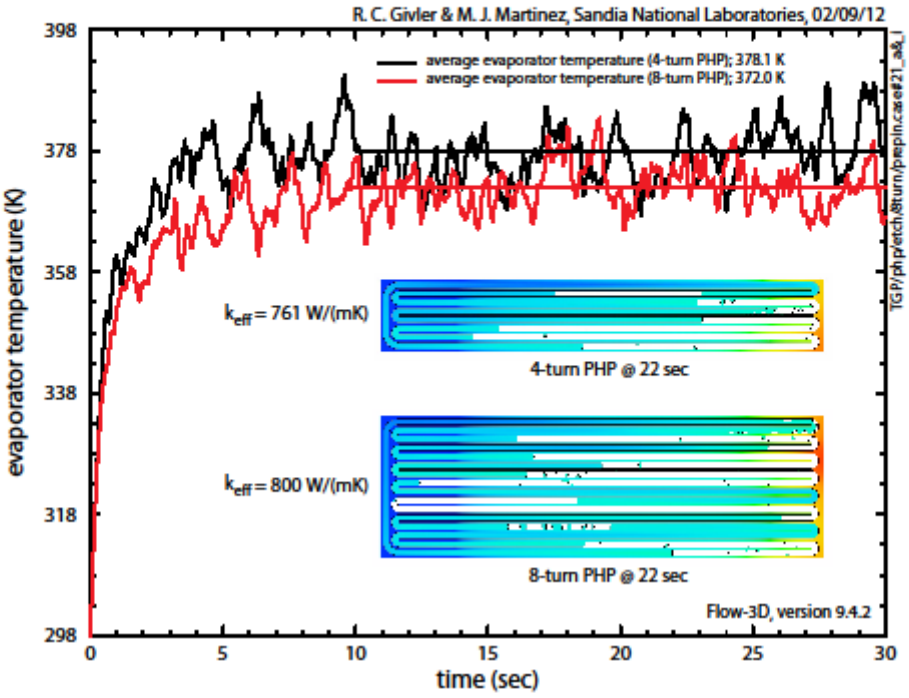

Figure 5: 2D, 4- and 8-turn PHP simulation results.

Figure 5. 2D, 4- and 8-turn PHP simulation results.

demonstrated by the 2D, 4-turn, PHP model the observed pulsation of liquid slugs and vapor bubbles is very similar to its 3D counterpart. The top inset in Figure 5 illustrates the physical configuration of the 2D, 4-turn PHP at a time corresponding to 22 s after initiation; temperature color scale for this contour plot ranges between 298 K (blue) < T < 390 K (red). While precise agreement between 2D and 3D models was neither anticipated nor demonstrated we believe that the results from the 2D model are representative of device performance and can serve as a baseline of comparison among other 2D model instances. Figure 5 also documents the performance of an 8-turn PHP; its performance is characterized with a value for k_{eff} = 800 W/(mK). This value is only slightly higher than the 4-turn version of the PHP indicating that doubling the number of channel turns from four to eight only marginally increases device efficiency. The non-steady evaporator temperature is plotted in red with its 'average temperature' (again obtained from three separate edge locations) calculated as 372.0 K. For comparison, the arrangement of liquid slugs and vapor bubbles within the device after 22 s of operation is illustrated in the bottom figure inset. This snapshot is representative of the device configuration during operation (10 s < t < 30 s). It appears that most of the liquid congregates toward the condenser side of the device with an occasional isolated foray through the evaporator. Again, all parameter settings for both cases featured in Figure 5 were the same with the exception made to the geometry for the number of turns. Power density supplied to the evaporator was 441 MW/m^3. The device heat load is 132 W/cm^2.

3.3 Effect of Evaporator Power

This section investigates the changes to efficiency of a 4-turn PHP in response to varying evaporator power. Figure 6 displays results for the 2D base geometry, in which the evaporator is uniformly heated with 0.64 W total power (34 W/cm^2 device heat load). For comparison this value is one-fourth that used for the base case discussed in Section 3.2. The figure inset shows the device layout with dimensions (in cm) of the various components. The figure inset also displays the initial configuration (*i.e.* initial liquid priming) of the model; elongated blue segments indicate those portions of the serpentine channel initially filled with liquid. We find that the quasi-steady results are not dependent on the initial configuration of liquid. Once the chaotic pulsating motion is established any imprint of the initial distribution of liquid is erased. This is beneficial because in practice the initial configuration of fluids would be very difficult to control. Initial liquid fill fraction is 0.63. The device is, again, oriented such that gravity acts toward the evaporator (bottom-heated). Three colored traces record the evaporator temperature as a function of time. The location of each trace is defined by its color that corresponds to the colored dot located on the evaporator shown in the figure inset. The 'average temperature' computed on the quasi-steady interval (10 s < t < 30 s) is 320.2 K and this value, in turn, is used to calculate an effective thermal conductivity of 685 W/(mK).

Additional information regarding device operation is provided in the form of a pressure trace (also illustrated in Figure 6). This value of pressure is recorded (either liquid or vapor) at a fixed location within the channel confines at the evaporator end of the model (see black dot in the figure inset). For an evaporator power of 0.64 W the nominal operating pressure recorded in Figure 6 (right side scale) is about 7200 Pa; this value for the liquid/vapor pressure can be used to estimate the quasi-steady temperature of the working media. Using the results presented in Figure 3 one can estimate the average media temperature to be 310 K at this location; this

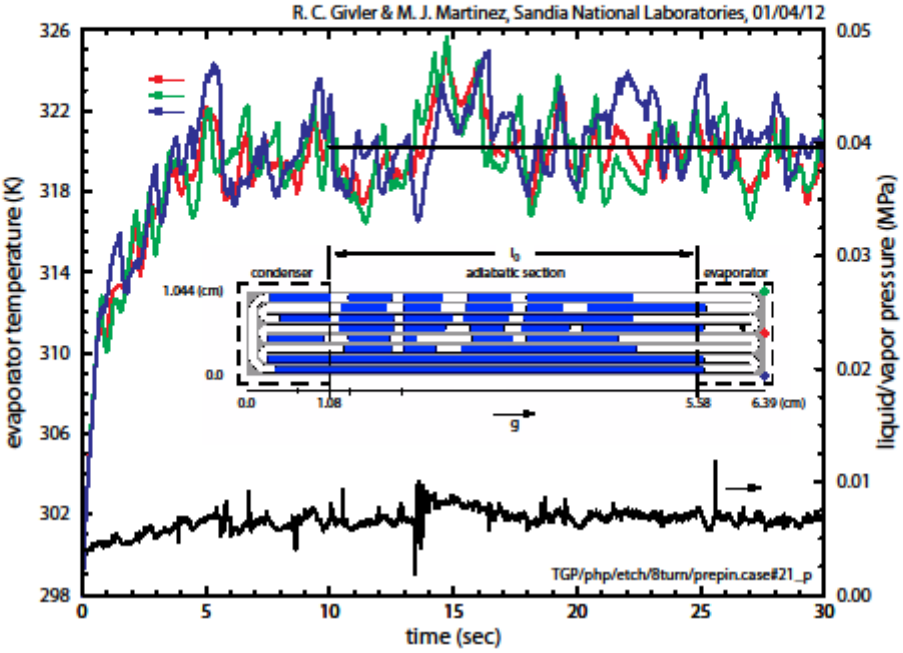

Figure 6: 2D, 4-turn PHP simulation results for reduced evaporator power, 0.64 W.

Figure 6. 2D, 4-turn PHP simulation results for reduced evaporator power, 0.64 W.

temperature is less than the average evaporator temperature but greater than that of the condenser. The spikes in the recorded pressure readings are most likely associated with localized boiling events. For comparison the same 2D, 4-turn PHP model is exercised at a higher evaporator power of 7.5 W (399 W/cm^2). This represents more than a 10-fold increase in evaporator heating from the case discussed previously. The results for this case of elevated heating are illustrated in Figure 7. Locations of the traces for both the evaporator temperatures and the channel pressure are the same as discussed for Figure 6. Note the elevated temperatures recorded in the evaporator; the 'average temperature' is computed to be 536.9 K. The corresponding value for the effective thermal conductivity is 752 W/(mK). This represents a modest 10% increase in efficiency compared to the less heated evaporator results presented in Figure 6. Pressure traces indicate that the average pressure of the working media (10 s < t < 30 s) is about 65,000 Pa and that value yields a corresponding temperature for the working media of 360 K at that location. Again, as anticipated, the value of this temperature prediction is between evaporator/condenser extremes but is closer to the condenser temperature.

Another observation can be made by comparing evaporator temperature traces for the different cases of applied evaporator power. It is clear that the frequency of oscillation for the evaporator temperature increases with power input. This has been confirmed with spectral analysis of the evaporator temperature traces recorded in Figures 6 and 7. Cycling of the evaporator temperature is directly related to the movement of liquid slugs through the evaporator. Higher heating rates associated with the results of Figure 7 impart a higher pulsating rate through the evaporator channel. This, again, has been confirmed by comparing animations of the rendered simulations. Figure 8 summarizes the efficiency of a 2D, 4-turn PHP in response to evaporator heating rate. Initially for low values of the evaporator power the effective thermal conductivity increases with increasing evaporator power, thus, the model predicts a more efficient device at higher evaporator power. However, this trend changes at 3 W of power delivered to the evaporator. Beyond this value for the heating rate the model predicts no increase in PHP performance. While, the definitive reason for this change in model behavior is not known it is speculated that the partition of heat transfer via conduction in the substrate walls is beginning to dominate the amount of heat transferred via the working media (both sensibly and by evaporation). This situation could arise at high evaporative powers if the evaporator and condenser are undersized, thereby limiting the amount of heat that can be transferred by the working media at both evaporator and condenser. This possibility was not investigated with the current model, but should be the topic of future work.

3.4 Initial Fill Ratio

One question that is often asked when discussing PHP behavior for closed systems is the value of the initial liquid fill fraction, x_{liq}, that produces optimal efficiency for a given device. The model developed here allows us to investigate this question. Intuition helps one to postulate the existence of an optimal fill ratio. Consider the two limiting cases: the device is empty (filled with vapor) or full (filled with liquid). In either case the efficiency of the device is determined strictly by conduction (assume motionless vapor or liquid). Here, there will be heat transfer by conduction from evaporator to condenser through both the substrate walls and also through the vapor or liquid that fills the channel. Both of these limiting situations will produce modest

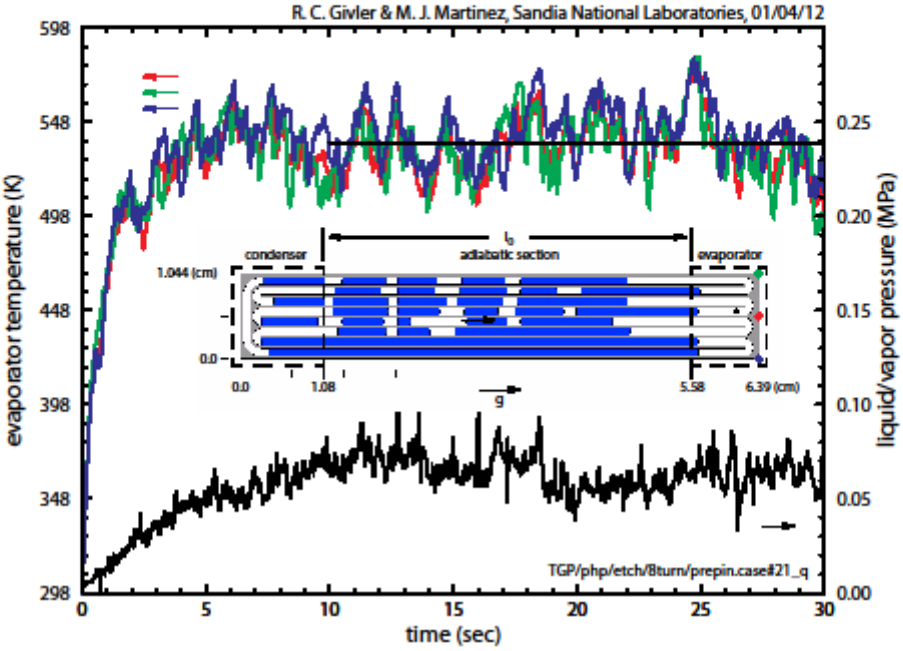

Figure 7: 2D, 4-turn PHP simulation results for increased evaporator power, 7.5 W.

Figure 7. 2D, 4-turn PHP simulation results for increased evaporator power, 7.5 W.

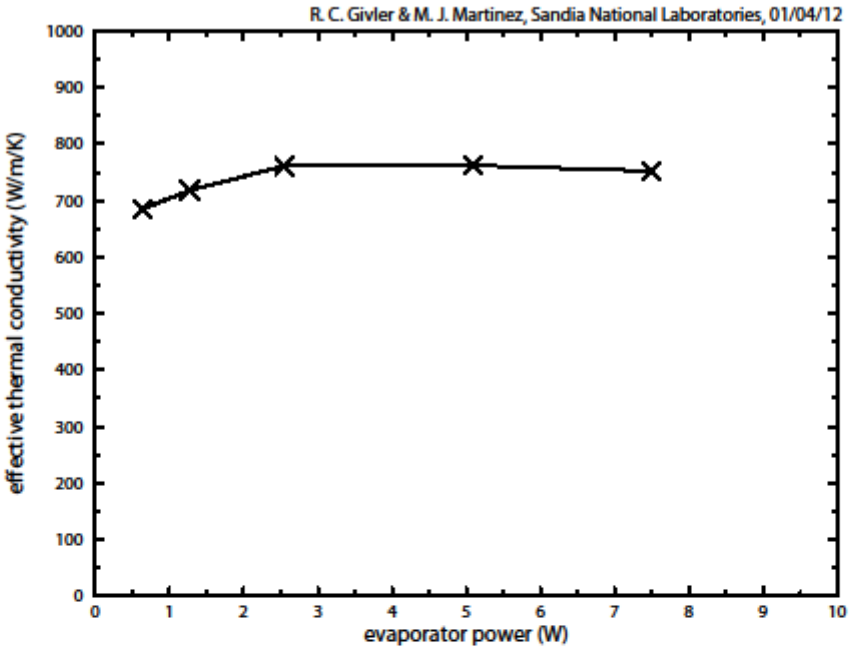

Figure 8: 2D, 4-turn PHP efficiency vs. evaporator power.

Figure 8. 2D, 4-turn PHP efficiency vs. evaporator power.

efficiencies owing to the low thermal conductivities exhibited by both water and its vapor as well as the limited cross-sectional area for heat transfer by conduction through the substrate walls. One might anticipate that any combination of water and its vapor, producing motion typical of an operating PHP, will enhance the overall device performance. Thus, one can reason that an optimal liquid fill fraction does exist.

Figure 9 displays results for a series of simulations using the baseline 2D, 4-turn PHP model. The initial liquid fraction spans the domain [0,1]. Effective thermal conductivity values for the curve endpoints correspond to steady conduction solutions for empty (vapor filled), k_{eff} = 90 W/(mk), and full (liquid filled), k_{eff} = 105 W/(mK), cases, respectively. Other data points representing effective thermal conductivities were calculated from transient simulations of the 2D, 4-turn PHP model. A maximum value for the effective thermal conductivity, k_{eff} = 843 W/(mK), corresponds to an initial liquid fraction, x_{liq} = 0.84. The shape of the curve in Figure 9 indicates that for this specific PHP model, efficiency is vastly improved (compared to conduction only behavior) for a broad range of liquid fill fractions ($0.2 < x_{liq} < 0.92$) and best in the neighborhood of x_{liq} = 0.85. The broad plateau demonstrated by the curve in Figure 9 indicates that model efficiency is high for a broad range of liquid fill fractions. In practical terms, the results illustrated in Figure 9 mean that good device performance can be achieved without precise initial priming.

3.5 Orientation Effects

Thus far, simulation results have been presented for models oriented with the gravity vector directed toward the evaporator, *i.e.* the so-called ‘bottom-heated’ configuration. In this instance the body force tends to move liquid toward the evaporator. Once there, it boils, promotes circulation and thereby increases the transfer of sensible heat from evaporator to condenser. Intuition suggests that a ‘bottom-heated’ orientation is advantageous since the body force is always acting to supply the evaporator with liquid. In this section we explore the consequences of ‘top-heating’, *i.e.* the gravity vector is directed toward the condenser.

Numerical results using the baseline geometry (2D, 4-turn PHP) and nominal parameter settings have served as a benchmark for each of the Figures 5-9. These comparative results have been used to quantify certain aspects of model performance, however, they do not help one fully appreciate the complicated dynamical behavior that occurs within an operating PHP. Animations of the dynamics have proved invaluable for revealing the complex dynamical motion of the liquid and vapor phases. An animation of the baseline case shows that the liquid/vapor motion is rather vigorous; nominal velocities are in the range of 1 m/s. The macroscopic motion is predominately oscillatory and not circulatory. Liquid motion throughout the model is extensive; in many instances the same liquid slug is observed to circulate from the evaporator through the condenser and back. This causes the spatial distribution of the liquid phase within the overall geometry to be nearly uniform (in a time-averaged sense). In other words, there is no preferential pooling of liquid either in the evaporator or condenser. Bubble nucleation events (predicted with a cavitation sub-model) are sudden and originate within the evaporator boundaries sometimes producing stray droplets. These fragments are subsequently absorbed by approaching liquid slugs. Peak evaporator temperature reached 393K with an average temperature calculated to be

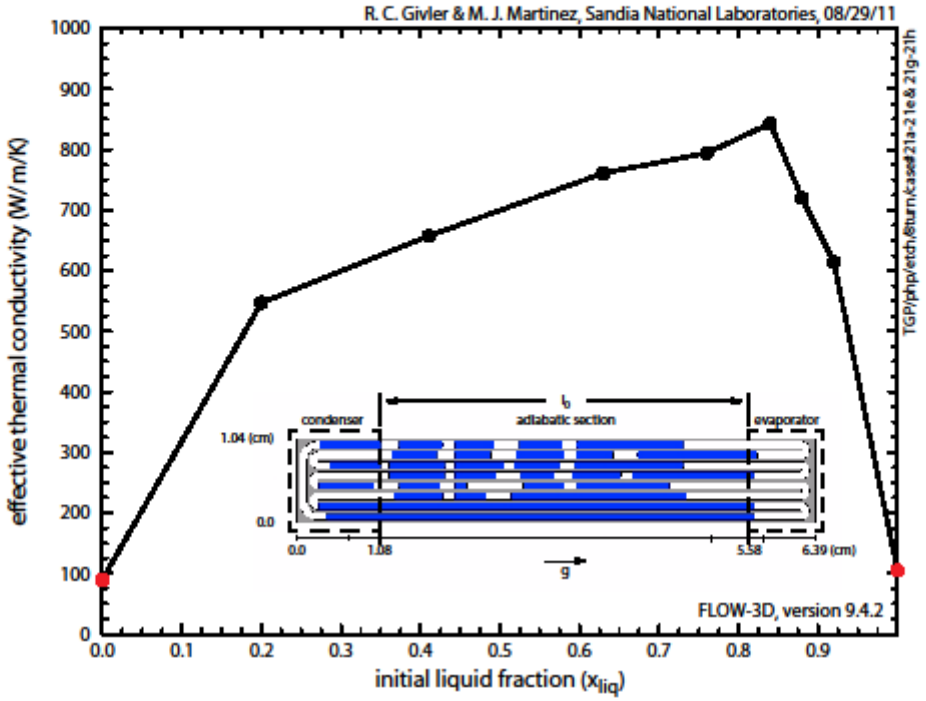

Figure 9: Predicted thermal performance for a 2D, 4-turn, bottom-heated PHP with varying liquid-fill fraction.

Figure 9. Predicted thermal performance for a 2D, 4-turn, bottom-heated PHP with varying liquid-fill fraction.

378K. The latter value was used to compute an effective thermal conductivity, k_{eff} = 761 W/(mK).

To investigate the effects of orientation, the baseline case is considered with the gravity direction reversed (top-heated). These model results have identifiable differences compared to those discussed previously. Liquid motion is less vigorous and of shorter displacement. Most noticeable is the bias in liquid distribution toward the condenser side of the model during PHP operation. Boiling of the liquid still occurs but takes place on the walls of the adiabatic section. Little liquid actually circulates through the evaporator channels save the occasional, isolated boiling event. This aggregate flow behavior causes the peak evaporator temperature to rise to 457K; the average temperature for the evaporator also rises and is calculated to be 426K. A consequence of this rise in evaporator temperature is a corresponding reduction in device efficiency, k_{eff} = 143 W/(mK). This value is only 50% higher than the efficiencies calculated for the conduction-only limits associated with Figure 9. Hence, it is apparent that most of the heat transferred in this model is by conduction via the channel walls. Heat transferred by forced convection contributes only modestly toward the overall efficiency of the device.

Continuing with this investigation, we analyzed a second 'top-heating' case subjected to a body force of 2g. Here, the effect of the increased body force is evident in the distribution of the liquid phase during PHP operation. Nearly all of the liquid phase collects toward the condenser side of the model. An occasional boiling event temporarily cools the evaporator and rearranges the liquid phase, but the system quickly returns to its almost perfectly gravity-segregated state. The peak evaporator temperature was recorded to be 472K and its average temperature was calculated to be 466K. For comparison, the thermal efficiency of the model is computed to be k_{eff} = 130 W/(mK). This value is also very close to the conduction-only limit demonstrated in Figure 9 for a liquid filled system, *i.e.* k_{eff} = 105 W/(mK). It is apparent from these findings that the strong body force directed toward the condenser has diminished the benefits afforded from a working PHP. It should be noted that these conclusions are applicable to the specific model designs investigated in this paper. More work should follow if these conclusions are to be broadened.

Deleterious effects of orientation with respect to gravity were also reported by Khandekar *et al.* (2003b), and Khandekar & Groll (2004) for tubular PHPs, showing marked decreases in performance between bottom-heated versus horizontal orientations. However our findings are in contradiction to Thompson *et al.* (2011b) who reported experiments on a prototype PHP, of similar design to our model, with no reduction in efficiency over large variations in gravity (using a spin-table) directed toward the condenser (top-heated).

3.6 Influence from a Tesla-type Valve

Animations of the simulations show that the dynamic flow patterns that develop within a functioning PHP are dominated by chaotic oscillations. Because of the random back-and-forth motion one can assume that some energy is dissipated by changing the direction of fluid momentum from one boiling event to the next. It seems as though some benefit could be gained if the flow was coaxed into becoming more circulatory in character, as was determined by

Akachi (1990) in a tubular PHP. Recent researchers have investigated this notion with the introduction of a diode into the flow path (Bardell, 2000, Thompson, *et al*., 2011c). In this section we add a single Tesla-type valve (*i.e.* check valve) to the baseline geometry to study its effect on PHP performance. These check valves are unique in that they have no moving parts. Characteristics of this Tesla-type valve were not optimized with regard to diodicity. Moreover, it is assumed that the check valve is less effective for two-phase flow. Therefore, the valve was strategically positioned in the condenser section of the PHP, where most of the time it remains completely filled with liquid.

The inset geometries of Figure 10 show the baseline model (top) and its modification to include a check valve (bottom). These images also depict the initial liquid fill fraction for each model which was set to $x_{liq} = 0.84$; all other parameter settings for both cases correspond to the nominal values of the baseline model. The horizontal velocity traces plotted in Figure 10 indicate the direction of flow in the top leg of the continuous, serpentine channel. The specific location is indicated by a colored dot; black for the baseline model and red for the check valve model. For the latter case the sign of the x-velocity component, *u*, indicates the direction of flow through the check valve. Its preferred direction (as determined by the configuration of the Tesla valve and the pressure drop across the valve) will produce velocities in the +x direction. It is instructive to compute the time-average value of *u*, *viz.* $\bar{u}$, for both cases. For the baseline model this value is +1.8 m/s. Because of the geometric symmetry intrinsic to this model one might have expected a value of $\bar{u}$ near zero, *i.e.* equal flow in both directions in this leg of the channel. The bias toward a positive value for the average velocity is probably caused by the body force, which, in both of these cases, is directed toward the evaporator.

Alternatively, the check valve model exhibits an average velocity of +6.2 m/s as calculated at the position indicated by the red dot. This indicates that the action of the check valve is indeed biasing the flow toward the +x direction. This bias toward flow circulation can be seen in the values calculated for overall thermal efficiencies. In the baseline model case $k_{eff} = 843$ W/(mK); this value increases to $k_{eff} = 866$ W/(mK) for the check valve model. We believe that the use of check valves could be exploited for gains in thermal efficiencies, if, for example, a properly designed check valve was attached to each leg of the serpentine channel and positioned in the condenser region.

3.7 PHP using Acetone

One final simulation was performed with the baseline model using acetone as the working fluid. Liquid slug motion was considerably more vigorous when compared to the baseline case using water. Also, the boiling events occurring in the evaporator were more frequent and violent. These observations can be expected owing to the higher vapor pressure generated by the acetone system for similar operating temperatures (see the respective curves for water and acetone in Figure 3). Despite the increase in fluid activity, the thermal performance for this case was not as good as that for the water-filled system. Average evaporator temperature reached 424 K yielding a value for $k_{eff} = 144$ W/(mK). The reduction in thermal performance may be explained by the difference in material properties (see Table 1) between the acetone and water systems. Acetone has less than half the thermal capacitance of water, half the dynamic viscosity and one-fourth the

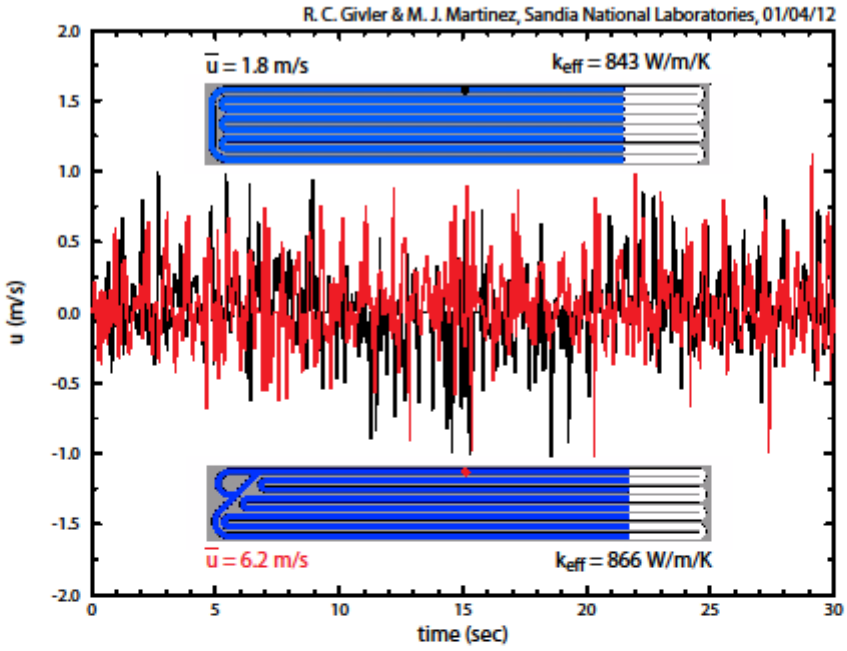

Figure 10: Simulation results for a 2D, 4-turn PHP with and without a Tesla-type valve.

Figure 10. Simulation results for a 2D, 4-turn PHP with and without a Tesla-type valve.

Table 3. Effective thermal conductivites over simulation matrix

Dimension	No. of turns	medium	Heat load (W/cm^2)	Liquid Fill Ratio (%)	Orientation	k_{eff} (W/mK)
3D	4	water	234	63	+g	1140
2D (baseline)	4	water	135	63	+g	761
	8	water	132	63	+g	800
	4	water	34	63	+g	685
	4	water	399	63	+g	752
	4	water	135	0	+g	90
	4	water	135	84	+g	843
	4	water	135	100	+g	105
	4	water	135	63	-g	143
	4	water	135	63	-2g	130
	4	acetone	135	63	+g	144

value for latent heat. Each of these differences contributes to an acetone system that boils quicker, flows faster but transports less sensible heat than a similar model filled with water.

The findings resulting from the parametric study are summarized in Table 3 for completeness. Here, the thermal performance of various PHPs is catalogued by using the measure of effective thermal conductivity. Parameter values that depart from those of the baseline case are highlighted in red. This table is particularly handy for quick comparison of results from the parametric study discussed in Section 3.

4. CONCLUSIONS

We have presented a new PHP model which, for the first time, includes most of the macro-level, physical processes important to the operation of flat plate PHPs (*e.g.* segregated two-phase flow, bubble nucleation, liquid slug coalescence, evaporation/condensation , conjugate heat transfer). The model still lacks from a precise knowledge of certain parameters relating to the boiling phenomena (existence of thin films) and conjugate heat transfer (values for h_{sl} and h_{sv}). Overall the effort, here, has produced a system-level tool to assess the performance of an operating PHP. The model both qualitatively and quantitatively predicts PHP performance characteristics and metrics, which can be compared directly to experimental measurements. This was demonstrated, in some instances, by favorable comparisons with experimental results on similar configurations. Application of the model also corroborated many previous performance observations with respect to key parameters such as heat loading, fill ratio and device orientation. This study imparts confidence that we are close to a PHP simulation tool that can be used for device evaluation and especially for providing insight into the behavior of these unusual heat transfer devices.

5. REFERENCES

Akachi, H., Structure of a Heat Pipe, U.S. Patent 4,921,041 (1990).

Akachi, H., F. Polasek, and P. Stulc, Pulsating Heat Pipes, *Proc. 5th International Heat Pipe Symposium*, Melbourne, Australia (1996) 208–217.

Bardell, R.L., The Diodicity Mechanism of Tesla-Type No-Moving-Parts Valves, Ph. D. Dissertation, University of Washington, United States (2000).

Callen, H.B., *Thermodyamics*, John Wiley & Sons, New York (1960).

Flow Science, Inc., *FLOW-3D User Manual,* Santa Fe, NM (2007).

Givler, R.C. and M.J. Martinez, Modeling of Pulsating Heat Pipes, Sandia National Laboratories technical report, SAND2009-4520, August (2009)

Hirt, C.W. and B.D. Nichols, Volume of fluid (VOF) method for the dynamics of free boundaries, Journal of Computational Physics **39**(1) (1981) 201–225.

Hirt, C.W., Modeling phase change and homogeneous bubbles, Technical Note FSI-01-TN57, Flow Science Inc., Santa Fe NM (2001).

Khandekar, S., M. Schneider, P. Schafer, R. Kulenovic, and M. Groll, Thermofluid dynamic study of flat-plate closed-loop pulsating heat pipes, *Microscale Thermophysical Engineering*, **6** (2002) 303-317.

Khandekar, S. and M. Groll, An insight into thermo-hydrodynamic coupling in closed-loop pulsating heat pipes, *International Journal of Thermal Sciences*, **43** (2004) 13-20.

Khandekar, S., N. Dollinger, and M. Groll, Understanding operational regimes of closed loop pulsating heat pipes: an experimental study, *Applied Thermal Engineering*, **23** (2003a) 707-719.

Khandekar, S., P. Charoensawan, M. Groll and P. Terdtoon, Closed loop pulsating heat pipes Part A: parametric experimental investigations, *Applied Thermal Engineering*, **23** (2003b) 2009-2020.

Khandekar, S., P. Charoensawan, M. Groll and P. Terdtoon, Closed loop pulsating heat pipes Part B: visualization and semi-empirical modeling, *Applied Thermal Engineering*, **23** (2003c) 2021-2033.

Ma, H.B., C. Wilson, Q. Yu, U.S. Choi and M. Tirumala, An experimental investigation of heat transport capacity in a nanofluid oscillating heat pipe, *ASME Journal of Heat Transfer*, **128** (2006a) 1213-1216.

Ma, H.B., B. Borgmeyer, C. Wilson, H. Park, Q. Yu, M. Tirumala and S. Choi, Nanofluid effect on the heat transport capability in an oscillating heat pipe, *Applied Physics Letters*, **88**(14) (2006b) 143116(1-3).

Miyazaki, Y., and H. Akachi, Heat Transfer Characteristics of Looped Capillary Heat Pipe, *Proc. 5th International Heat Pipe Symposium*, Melbourne, Australia, (1996) 378–383.

Miyazaki, Y., and H. Akachi, Self Excited Oscillation of Slug Flow in a Micro Channel, *Proc. 3rd International Conference on Multiphase Flow*, Lyon, France, June 8–12 (1998).

Nikolayev, V. S., A dynamic film model of the pulsating heat pipe, *ASME Journal of Heat Transfe*r, **133**(8), Article Number 081504 (August 2011).

Osher, S., and S. Fedwick, *Level Set Methods and Dynamic Implicit Surfaces*, Springer, New York (2003).

Cheng, P., H-Y. Wu and F-J. Hong, Phase-change heat transfer in microsystems, *Journal of Heat Transfer*, **129** (2007), 101-107.

Plesset, M.S. and A. Prosperetti, Bubble dynamics and cavitation, Annual Reviews of Fluid Mechanics, **9** (1977) 145-185.

Qu, W. and H.B. Ma, Theoretical analysis of start-up of a pulsating heat pipe, *International Journal of Heat and Mass Transfer*, **50** (2007) 2309-2316.

Sethian, J.A., *Level Set Methods and Fast Marching Methods: Evolving Interfaces in Computational Geometry, Fluid Mechanics, Computer Vision, and Material Science*, Cambridge Univ. Press, Cambridge, U.K., (1999).

Shafii, M.B., A. Fahgri, and Y. Zhang, Thermal modeling of unlooped and looped pulsating heat pipes, *Journal of Heat Transfer*, **123** (2001) 1159-1172.

Thompson, S.M., P. Cheng and H.B. Ma, An experimental investigation of a three-dimensional flat-plate oscillating heat pipe with staggered microchannels, *International Journal of Heat and Mass Transfer*, **54** (2011a) 3951-3969.

Thompson, S.M., A.A. Hathaway, C.D. Smoot, C.A. Wilson, H.B. Ma, R.M. Young, L. Greenberg, B.R. Osick, S. Van Campen, B.C. Morgan, D. Sharar, N. Jankowski, Robust thermal performance of a flat-plate oscillating heat pipe during high-gravity loading, *ASME Journal of Heat Transfer*, 133, Article Number 104504 (2011b).

Thompson, S.M., H.B. Ma and C. Wilson, Investigation of a flat-plate oscillating heat pipe with Tesla-type check valves, Experimental Thermal and Fluid Science, **35** (7) (2011c) 1265-1273.

Wilson, C., B. Borgmeyer, R.A. Winholtz, H.B. Ma, D.L. Jacobson, D.S. Hussey, and M. Arif, Visual observation of oscillating heat pipes using neutron radiography, *Journal of Thermophysics and Heat Transfer*, **22** (3) (2008) 366-372.

Yuan, D., W. Qu, and T. Ma, Flow and heat transfer of liquid plug and neighboring vapor slugs in a pulsating heat pipe, *International Journal of Heat and Mass Transfer*, **53** (2010) 1260-1268.

Zhang, Y., A. Faghri, Heat transfer in a pulsating heat pipe with open end, *International Journal of Heat and Mass Transfer*, **45** (2002) 775-764.

Zhang, Y., A. Fahgri, and MB Shaffii, Analysis of liquid-vapor pulsating flow in a U-shaped miniature tube, *International Journal of Heat and Mass Transfer*, **45** (2002) 2501-2508.

Zhang, Y. and A. Faghri, Oscillatory flow in PHPs with arbitrary number of turns, *Journal of Thermophysics & Heat Transfer*, **17**(3) (2003) 340.

Zuo, Z. J., M.T. North and L. Ray, Combined Pulsating and Capillary Heat Pipe Mechanism for Cooling of High Heat Flux Electronics, Proc. ASME Heat Transfer Device Conference, pp. 2237–2243, Nashville, Tennessee, USA, (1999).

Zuo, ZJ, M.T. North and K.L. Wert, High heat flux heat pipe mechanism for cooling of electronics, IEEE Transactions of components and packaging technologies, **24**(2) (2001) 220-225.

DISTRIBUTION

1 Dr. Lawrence Greenberg (electronic copy)
Lawrence.greenberg@ngc.com
Northop Grumman Electronic Systems
P.O. Box 1693
Baltimore, MD 21203

1 Dr. Don Mullin (electronic copy)
Donald.mullin@navy.mil
SPAWARSYSCEN 55430
53570 Silvergate Ave RM 3203
San Diego, CA 92152-5287

1 Dr. Avram Bar-Cohen (electronic copy)
avram.bar-cohen@darpa.mil
DARPA/MTO
3701 N. Fairfax Ave.
Arlington, VA 22203

1 Dr. Jennifer Korzeniowski (electronic copy)
Jennifer.Korzeniowski.ctr@darpa.mil
DARPA/MTO
3701 N. Fairfax Ave.
Arlington, VA 22203

1	MS0828	S. N. Kempka	1510 (electronic copy)
1	MS0828	M. Pilch	1514 (electronic copy)
1	MS0836	R. C. Givler	1514 (electronic copy)
1	MS0836	M. J. Martinez	1514 (electronic copy)
1	MS0899	Technical Library	9536 (electronic copy)


Sandia National Laboratories